Automatic branch detection of the arterial system from abdominal aortic segmentation

Sébastien Riffaud, Gwladys Ravon, Thibault Allard, Florian Bernard, Angelo Iollo, Caroline Caradu

Medical & Biological Engineering & Computing manuscript No.
(will be inserted by the editor)

Automatic branch detection of the arterial system from abdominal aortic segmentation

Sébastien Riffaud · Gwladys Ravon · Thibault Allard · Florian Bernard · Angelo Iollo · Caroline Caradu

Received: date / Accepted: date

Abstract We present a new method to automatically identify the different arteries present in an abdominal aortic segmentation. In this approach, the arterial system is first represented by a vascular tree, extracted from the segmentation and containing the topologic and geometric features (branch position, branch direction, branch length, branch diameter) of the arterial system. Then, the branches of the vascular tree are matched with the main arteries originating from the aorta: celiac artery, superior mesenteric artery, renal arteries and common iliac arteries. This match is determined by maximizing a similarity measure between the different branches and corresponding arteries. We evaluate this method on 239 segmentations obtained from 102 different patients. The results demonstrate the accuracy of the proposed method, capable of delivering an error of less than 2.5% for the identification of the celiac and superior mesenteric arteries, 8.4% for the renal arteries, and 2.1% for the common iliac arteries.

Keywords Computed tomography · Abdominal aortic aneurysm · Automatic branch detection · Graph matching method · Aortic root

Sébastien Riffaud and Gwladys Ravon contributed equally to this work.

Sébastien Riffaud
Inria - Bordeaux Sud-Ouest, Team MEMPHIS, 33405 Talence, France
E-mail: sebastien.riffaud@inria.fr

Gwladys Ravon
Inria - Bordeaux Sud-Ouest, Team MEMPHIS, 33405 Talence, France

Thibault Allard
Nurea, 33000 Bordeaux, France

Florian Bernard
Nurea, 33000 Bordeaux, France

Angelo Iollo
IMB, UMR 5251, Université de Bordeaux, 33405 Talence, France
Inria - Bordeaux Sud-Ouest, Team MEMPHIS, 33405 Talence, France

Caroline Caradu
Vascular Surgery Department, Bordeaux University Hospital, 33000 Bordeaux, France

1 Introduction

Abdominal aortic aneurysm (AAA) is associated with a high mortality rate if not treated immediately after its rupture [6, 2]. Measuring geometric characteristics (length, diameter, volume) of an AAA is therefore vital in diagnostic assessment or surgical intervention planning. However, manual extraction of anatomical structures in an abdominal aortic segmentation is time consuming, requires a certain level of experience and can introduce inter-observer variations in the results.

Several methods have been proposed to automatically identify anatomical reference points (landmarks) commonly used in medical imaging analysis. In the works of Elattar [4] and Lalys [5], the authors proposed methods for locating landmarks on the surface of the aortic arch to facilitate the planning of transcatheter aortic valve implantation. These landmarks are used to find the sizing parameters of the prothesis. Both approaches rely on the centerline and segmentation of the aorta. However, they do not focus on the vascular region we are considering. In Tahoces [8], they developed a method to find similar landmarks and added the identification of the celiac artery. The superior mesenteric and principal renal arteries are also identified without the need to assume their presence. Closer to our problem, Dehmeshki [3] developed an AAA detection method. They look for AAAs between the celiac artery and the aortic bifurcation. After extracting the lumen, they identify an approximate position for the celiac artery as the end of the lung region. Bifurcating branches are separated from the main aorta using a projection in the sagittal view into one 2D image and morphological operations on the lumen segmentation. The first isolated branch from the top of the 2D image is then defined as the celiac artery. The aortic bifurcation is finally localized from the centerline using cluster connectivity and rule-based techniques. Oda [7] developed a more complete method since they label 14 upper and lower abdominal arteries. From the segmentation of the arterial system, they extract the centerline and deduce the vascular tree structure. The method then relies on rule-based methods, classifiers and correction process. The classifiers use features such as diameter, curvature and direction of the branches.

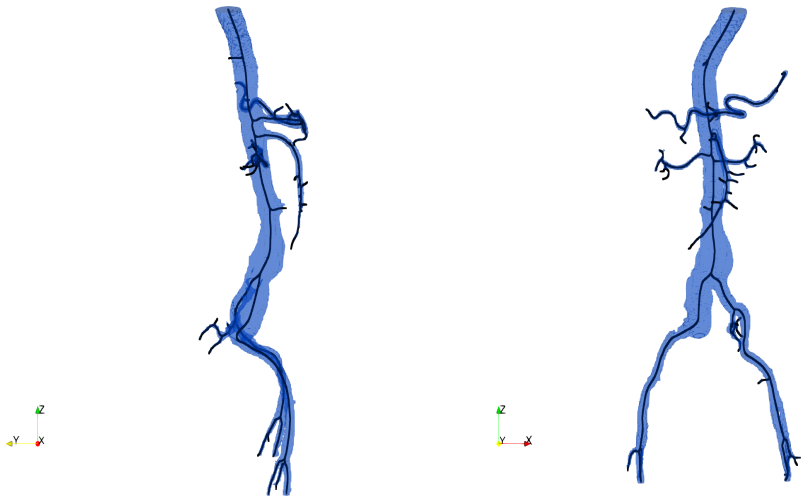

Fig. 1 Example of segmentation (blue) and vascular tree (black) obtained from tomography scan images.

This work aims to develop a new method to identify in a fully automatic way the different arteries present in an abdominal aortic segmentation. In this approach, the arterial system is first represented by the vascular tree extracted from the segmentation, as illustrated in Figure 1. The branches of the vascular tree are then matched with the main arteries originating from the aorta. In particular, we focus on the detection and identification of the celiac artery (CA), superior mesenteric artery (SMA), principal and polar renal arteries (RAs) and common iliac arteries (CIAs). Moreover, except for the CIAs, we do not need to assume the presence of the other arteries. The accuracy and robustness of the present method are finally demonstrated on a large dataset including 239 segmentations from 102 different patients.

2 Methodology

In order to annotate the branches of the vascular tree, our method proceeds in two steps. The first step employs a matching algorithm to identify the CA, SMA, a first left and right RAs, and the CIAs. In this approach, the branches that best match the different arteries originating from the aorta are determined by maximizing a similarity measure between the different branches and corresponding arteries. In the second step, a decision rule-based algorithm detects possible extra RAs to obtain the complete description of the arterial system. To this end, we extract the branches that have not already been matched, and decision rules are employed to determined whether these branches correspond to additional RAs or not.

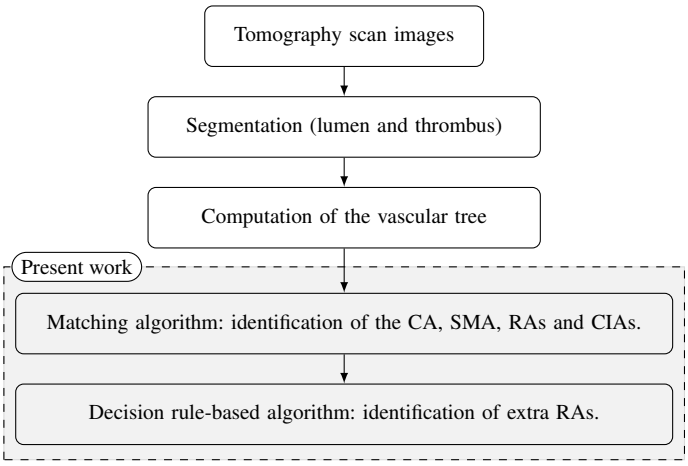

Fig. 2 Schematic diagram illustrating the automatic branch detection of the arterial system.

2.1 Dataset

The present work is restricted to segmentations that contain the aortic bifurcation. The study includes 239 segmentations from 102 different patients. Segmentations are obtained from pre-operative and post-endovascular aneurysm repair computed tomography scan images. These images contain the entire abdominal aorta and may extend to the aortic arch. In addition 24 segmentations present additional RAs for a total of 29 polar RAs.

The segmentations and vascular trees are provided by Nurea (`https://www.nurea-soft.com`) using the software PRAEVAorta [1]. This software employs deep learning approaches to automatically identify the voxels corresponding to lumen and thrombus in tomography scan images. The vascular tree is then extracted from the full segmentation, that is lumen and thrombus. This one corresponds to a tree (i.e. a connected acyclic undirected graph), where the nodes are located along the central lines of the segmentation and the edges represent the topology of the arterial system. In this way, the vascular tree contains the topologic and geometric features (branch position, branch direction, branch length, branch diameter) of the segmentation.

2.2 Matching algorithm

2.2.1 Notations and definitions

Before describing the matching algorithm, we need to introduce the definitions and notations used in the following.

Definition 1 ***(Graph path)*** *A sequence of vertices* $(v^1,\dots,v^n)$ *is a graph path if* $\{v^i,v^{i+1}\}$ *is an edge of the graph for* $i=1,\dots,n-1$.

Theorem 1 *Two vertices of a tree are connected by exactly one path.*

Definition 2 ***(Distance between two nodes)*** *Let* v^1 *and* v^n *be two vertices of the vascular tree. There exists a unique path* $(v^1,\dots,v^n)$ *connecting theses two vertices according to Theorem 1. The distance between* v^1 *and* v^n *is then defined as the sum of the Euclidean distances between two adjacent vertices of the path* $(v^1,\dots,v^n)$*:*

$$\mathrm{dist}(v^1,v^n)=\sum_{i=1}^{n-1}\left\|\mathbf{v}^{i+1}-\mathbf{v}^i\right\|_2,$$

where $\mathbf{v}^i=(v^i_x,v^i_y,v^i_z)^T\in\mathbb{R}^3$ *denote the spatial coordinates of vertex* v^i.

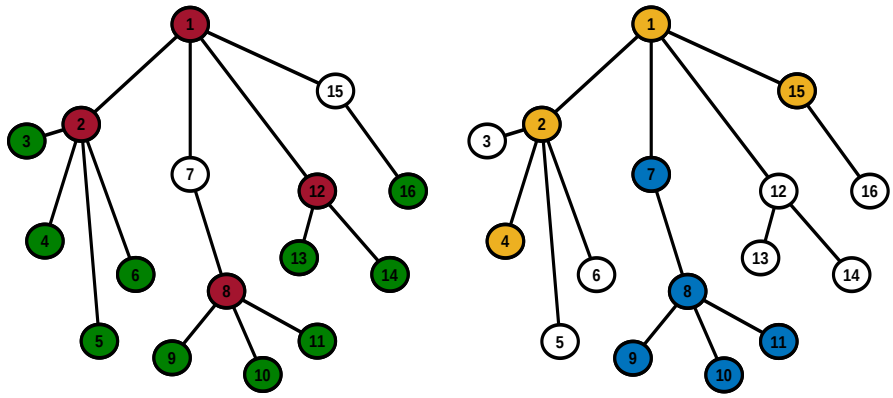

Fig. 3 Illustration of the different definitions: bifurcation nodes (red), leaf nodes (green), graph path between vertices 4 and 15 (yellow) and tree branch starting from node 7 and containing vertex 8 (blue).

Definition 3 ***(Leaf and bifurcation nodes)*** *In a tree, a leaf is a vertex with exactly one neighbour. Similarly, a bifurcation node is a vertex with at least three neighbours.*

Definition 4 ***(Tree branch)*** *The tree branch starting from the bifurcation node b and containing the vertex u^m is defined as the set of vertices $\{v^1,\dots,v^n\}$ such that the path between b and v^i contains the vertex u_1, where $(b,u_1,\dots,u^m)$ is the path connecting b and u^m.*

Definition 5 ***(Directions of a branch)*** *Let $\{v^1,\dots,v^n\}$ be the vertices of the branch starting from the bifurcation node b and containing the vertex u^m. The direction of this branch is defined as the vector with origin $\mathbf{b}$ that best approximates the vertices $\{v^1,\dots,v^n\}$. More precisely, considering the matrix*

$$\mathbf{A} = \begin{pmatrix} v_x^1 - b_x & v_y^1 - b_y & v_z^1 - b_z \\ v_x^2 - b_x & v_y^2 - b_y & v_z^2 - b_z \\ \vdots & \vdots & \vdots \\ v_x^n - b_x & v_y^n - b_y & v_z^n - b_z \end{pmatrix} \in \mathbb{R}^{n\times 3} \tag{1}$$

and the eigenvector $\mathbf{e} \in \mathbb{R}^3$ associated with the largest eigenvalue of $\mathbf{A}^T\mathbf{A} \in \mathbb{R}^{3\times 3}$, the direction with origin $\mathbf{b}$ that best approximates vertices $\{v^1,\dots,v^n\}$ is given by

$$\mathbf{d}_{opt}(b,v^1,\dots,v^n) = \operatorname{sign}\left(\mathbf{1}^T\mathbf{A}\mathbf{e}\right)\mathbf{e},$$

where $\mathbf{1} = (1,\dots,1)^T \in \mathbb{R}^n$. The global direction of the branch starting from b and containing u^m is then defined as

$$\mathbf{d}_{glob}(b,u^m) = \mathbf{d}_{opt}(b,v^1,\dots,v^n).$$

Similarly, we define the local direction $\mathbf{d}_{loc}(b,u^m)$, representing the direction of the beginning of the branch (i.e. when the corresponding artery leaves the aorta). This direction is computed in the same way as the global direction except that only the vertices located at the beginning of the branch are used. More precisely, given the path $(b,n^1,\dots,n^k)$, where n^k denotes the first bifurcation or leaf encountered starting from b and going to u^1, we only consider the vertices $\{n^i\}_{i=1}^l \subset \{n^1,\dots,n^k\}$, such that n^i is at most $3r$ from b:

$$\operatorname{dist}(b,n^i) \leqslant 3r,$$

where r is the radius of the artery at node b. The local direction is then given by

$$\mathbf{d}_{loc}(b,u^m) = \mathbf{d}_{opt}(b,n^1,\dots,n^l).$$

Definition 6 ***(Angle between two directions)*** *Notably, the global and local directions allow to measure the angle of a branch with different anatomical directions. In particular, we will consider in the following the angle between two vectors $\mathbf{d}^1,\mathbf{d}^2 \in \mathbb{R}^3_*$ in the horizontal and frontal planes defined respectively by*

$$\operatorname{angle}_{x,y}(\mathbf{d}^1,\mathbf{d}^2) = \cos^{-1}\left(\frac{d_x^1 d_x^2 + d_y^1 d_y^2}{\sqrt{(d_x^1)^2 + \left(d_y^1\right)^2}\sqrt{(d_x^2)^2 + \left(d_y^2\right)^2}}\right)$$

and

$$\operatorname{angle}_{x,z}(\mathbf{d}^1,\mathbf{d}^2) = \cos^{-1}\left(\frac{d_x^1 d_x^2 + d_z^1 d_z^2}{\sqrt{(d_x^1)^2 + \left(d_z^1\right)^2}\sqrt{(d_x^2)^2 + \left(d_z^2\right)^2}}\right).$$

In case of vanishing denominator, the angle in the horizontal or frontal plane is replaced by the angle in 3D space:

$$\text{angle}(\mathbf{d}^1, \mathbf{d}^2) = \cos^{-1}\left(\frac{\left(\mathbf{d}^1\right)^T \mathbf{d}^2}{\|\mathbf{d}^1\|_2 \|\mathbf{d}^2\|_2}\right).$$

Definition 7 ***(Lengths of a branch)*** *Let $\left\{v^1, \ldots, v^n\right\}$ be the nodes of the branch starting from the bifurcation node b and containing the vertex u^m. The length of this branch is defined as the maximum distance between the bifurcation node b and the different nodes $\left\{v^1, \ldots, v^n\right\}$:*

$$\text{length}(b, u^m) = \max_{i \in \{1,\ldots,n\}} \text{dist}(b, v^i).$$

In addition, we also define the length of this branch in a direction $\mathbf{d} \in \mathbb{R}^3_*$:

$$\text{lengthD}\,(b, u^m, \mathbf{d}) = \frac{\|\mathbf{A}\mathbf{d}\|_\infty}{\|\mathbf{d}\|_2},$$

where the matrix $\mathbf{A}$ is given in Equation (1)*. In particular, we will consider in the next sections the branch lengths in the following anatomical directions:*

- *left to right:*

$$x^-(b, u^m) = \text{lengthD}\left(b, u^m, (-1,0,0)^T\right);$$

- *right to left:*

$$x^+(b, u^m) = \text{lengthD}\left(b, u^m, (1,0,0)^T\right);$$

- *posterior to anterior:*

$$y^-(b, u^m) = \text{lengthD}\left(b, u^m, (0,-1,0)^T\right);$$

- *superior to inferior:*

$$z^-(b, u^m) = \text{lengthD}\left(b, u^m (0,0,-1)^T\right);$$

- *inferior to superior:*

$$z^+(b, u^m) = \text{lengthD}\left(b, u^m, (0,0,1)^T\right).$$

2.2.2 Enumeration of valid pairings

The matching algorithm aims to find the branches of the vascular tree that best match the arteries located along the aorta. To this end, a branch is represented as a pair (u, v), where u denotes the bifurcation from which the branch originates and v denotes a node belonging to this branch. Since there are six branches to identify, a pairing is then defined as a set $\{(u^{ca}, v^{ca}), (u^{sma}, v^{sma}), (u^{lra}, v^{lra}), (u^{rra}, v^{rra}), (u^{lcia}, v^{lcia}), (u^{rcia}, v^{rcia})\}$, where each pair represents respectively the CA, MSA, left RA, right RA, left CIA and right CIA.

Bifurcation pairing. In order to enumerate every possible pairing, we first determine the nodes $(u^{ca},\dots,u^{rcia})$. As these nodes are located at the beginning of a branch, they either correspond to a bifurcation node or are left empty (i.e. $u=\varnothing$) in order to take into account the case where the associated artery is not present in the vascular tree. In addition, since the arteries of interest originate from the aorta, we consider only the bifurcation nodes located along the aorta. To this end, we exploit the fact that the aorta is the only artery connecting the part above the RAs with the part below the aortic bifurcation. The path between the highest and lowest nodes thus passes through the part of the aorta of interest, and we consider only the bifurcations $\{b^1,\dots,b^n\}$ located along this path, as illustrated in Figure 4. The nodes $(u^{ca},\dots,u^{rcia})$ finally belong to the set $\{\varnothing,b^1,\dots,b^n\}$ and since the same bifurcation b can be associated with several nodes u, there are $(n+1)^6$ possible pairings. However, in order to represent a valid pairing, the nodes $(u^{ca},\dots,u^{rcia})$ must satisfy the following anatomical constraints:

– the left and right CIAs start from the same bifurcation (i.e. the aortic bifurcation):

$$u^{lcia}=u^{rcia}; \tag{2}$$

– the bifurcation of the CA is above the bifurcation of the SMA and strictly above the bifurcations of the other arteries:

$$\begin{gathered} u_z^{ca}\geqslant u_z^{sma},\\ u_z^{ca}>u_z^{i}\quad \forall i\in\{lra,rra,lcia,rcia\}; \end{gathered} \tag{3}$$

– the aortic bifurcation is strictly below the bifurcations of the other arteries:

$$u_z^{lcia}=u_z^{rcia}<u_z^{i}\quad \forall i\in\{ca,sma,lra,rra\}; \tag{4}$$

– the distance between the bifurcations of the different arteries is lower than 250 millimetres (mm):

$$\mathrm{dist}(u^i,u^j)\leqslant 250\text{ mm}\quad \forall i,j\in\{ca,sma,lra,rra,lcia,rcia\}; \tag{5}$$

– the distance between the bifurcations of the CA, SMA and RAs is lower than 70 mm:

$$\mathrm{dist}(u^i,u^j)\leqslant 70\text{ mm}\quad \forall i,j\in\{ca,sma,lra,rra\}; \tag{6}$$

– if both the left and right RAs are present, then the distance between the two RAs is less than 35 mm:

$$u^{lra},u^{rra}\neq\varnothing\implies \mathrm{dist}(u^{lra},u^{rra})\leqslant 35\text{ mm}; \tag{7}$$

– if both the left and right RAs are present, then the bifurcation of the SMA is above the bifurcations of the lowest RA:

$$u^{lra},u^{rra}\neq\varnothing\implies \left(u_z^{sma}\geqslant u_z^{lra}\right)\vee\left(u_z^{sma}\geqslant u_z^{rra}\right); \tag{8}$$

– if there is only one RA, then the bifurcation of the SMA is at most 35 mm under this RA:

$$\begin{gathered} \left(u^{lra}\neq\varnothing\right)\wedge\left(u^{rra}=\varnothing\right)\implies \left(u_z^{sma}\geqslant u_z^{lra}\right)\vee\left(\mathrm{dist}(u^{sma},u^{lra})\leqslant 35\text{ mm}\right),\\ \left(u^{lra}=\varnothing\right)\wedge\left(u^{rra}\neq\varnothing\right)\implies \left(u_z^{sma}\geqslant u_z^{rra}\right)\vee\left(\mathrm{dist}(u^{sma},u^{rra})\leqslant 35\text{ mm}\right). \end{gathered} \tag{9}$$

These conditions involve three parameters: the maximum distance between the bifurcations of the different arteries (250 mm), the maximum distance between the bifurcations of the CA, SMA and RAs (70 mm) and the maximum distance between the RAs (35 mm). These parameters were chosen based on reference anatomic values and are consistent with the current dataset according to Table 1. In practice, uncertainties in these thresholds have a small influence on the accuracy of the method. For example, the maximum distance between the bifurcations of the different arteries is set to 250 mm; but if we had chosen 210 mm, the result would have been the same according to Table 1. We just need to make sure that these parameters are sufficiently large to not exclude valid cases while being small enough to eliminate outliers. Additionally, note that these thresholds could also be parameterized, with respect to patient size for example, in order to increase the robustness of the method to new datasets.

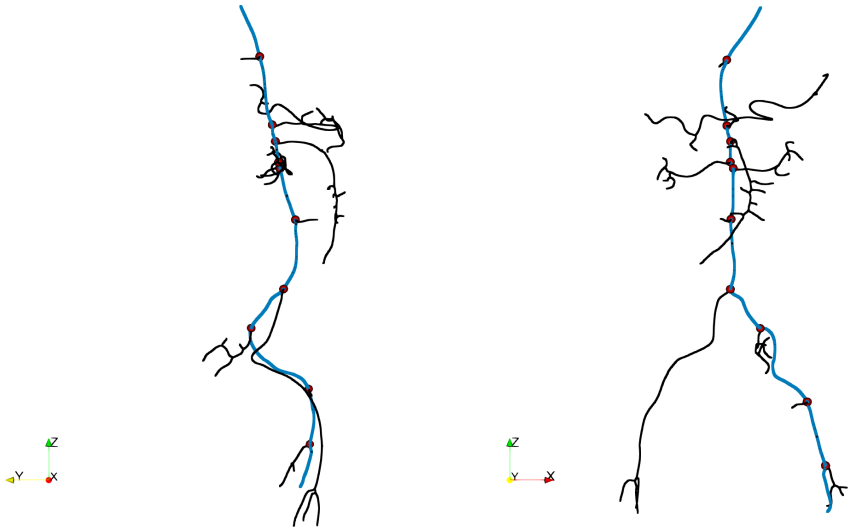

Fig. 4 Example illustrating the selection of valid bifurcation nodes: vascular tree (black), path between the lowest and highest nodes (blue) and valid bifurcation nodes (red).

	Mean	Standard deviation	Maximum
Maximum distance between the bifurcations of the different arteries	157.7 mm	19.2 mm	206.9 mm
Maximum distance between the bifurcations of the CA, SMA and RAs	35.0 mm	10.9 mm	68.7 mm
Maximum distance between the principal RAs	9.5 mm	5.1 mm	31.9 mm

Table 1 Statistics used to determine the parameters involved in conditions (2)-(9). These statistics were computed from the 239 segmentations of the dataset.

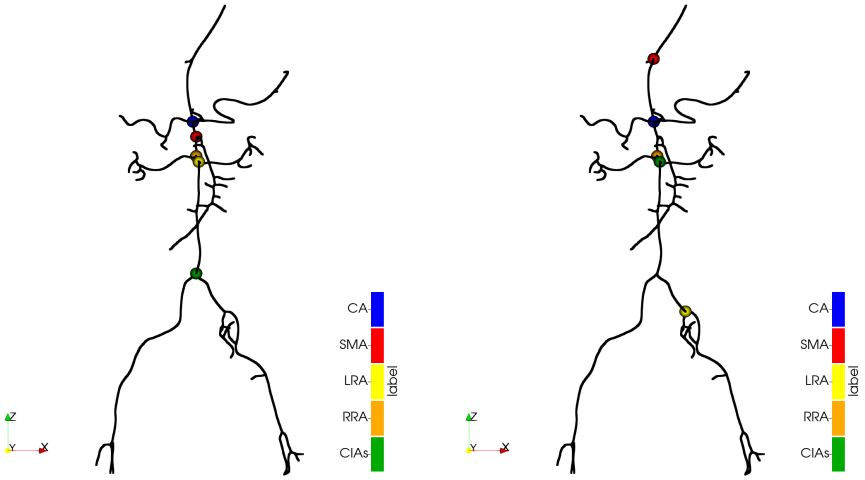

Fig. 5 Example of bifurcation pairing: valid bifurcation pairing (left) and invalid bifurcation pairing (right).

Branch pairing. Once $(u^{ca},\dots,u^{rcia})$ are fixed, we only have to determine $(v^{ca},\dots,v^{rcia})$. Each node v corresponds to a neighbour of u, and the pair (u,v) thus represents the branch starting from the bifurcation u and containing the node v. Moreover, as the branches associated with the arteries of interest are not part of the aorta, $(v^{ca},\dots,v^{rcia})$ corresponds to the neighbours of vertices $(u^{ca},\dots,u^{rcia})$ that do not belong to the aorta. To this end, let u^{max} and u^{min} be respectively the highest and lowest bifurcations of $(u^{ca},\dots,u^{rcia})$. We consider the neighbours of vertices $(u^{ca},\dots,u^{rcia})$ that do not belong to the path between u^{max} and u^{min}. In addition, we still need to remove the branch corresponding to the aorta that could be above u^{max}, as shown in Figure 6. To do this, if u^{max} has at least one neighbour whose corresponding branch is directed upwards, we remove the neighbour v^{max} associated to the branch with the largest radius, and thus corresponding to the aorta. In particular, let a branch starting from u^{max} and containing the neighbour w. The radius of this branch is defined as the mean radius of the nodes between u^{max} and the first bifurcation or leaf encountered starting from u^{max} and going to w. Finally, given the set of neighbours $\{n^1,\dots,n^m\}$ that do not belong to the aorta, the nodes $(v^{ca},\dots,v^{rcia})$ are a subset of $\{\varnothing,n^1,\dots,n^m\}$. However, in order to obtain a valid pairing, the nodes $(v^{ca},\dots,v^{rcia})$ must verify the following conditions:

– if u is left empty, then v is also left empty:

$$u^i=\varnothing \implies v^i=\varnothing \quad \forall i\in\{ca,sma,lra,rra,lcia,rcia\}; \tag{10}$$

– the nodes v associated with a branch are distinct in order to represent different branches:

$$\left(i\neq j\right)\wedge\left(v^i\neq\varnothing\right)\wedge\left(v^j\neq\varnothing\right)\implies v^i\neq v^j \quad \forall i,j\in\{ca,sma,lra,rra,lcia,rcia\}. \tag{11}$$

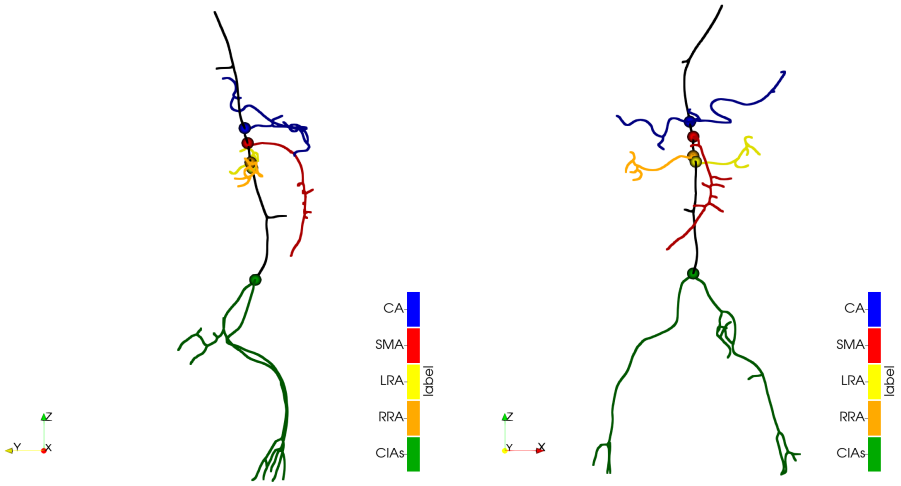

Fig. 6 Example of branch pairing: path between $u^{max} = u^{ca}$ and $u^{min} = u^{lcia} = u^{rcia}$ corresponding to the aorta (black) and branch (u^{max}, v^{max}) located above u^{max} which corresponds to the aorta (black).

2.2.3 Score evaluation

In order to find the branches of the vascular tree that best match the arterial system, a score is assigned to every valid pairing. This score measures the similarity between the different branches (u, v) and their corresponding arteries:

$$\begin{aligned}\text{score} = &\ \text{CAscore}(u^{ca}, v^{ca}) \\ &+ \text{SMAscore}(u^{sma}, v^{sma}) \\ &+ \text{LRAscore}(u^{lra}, v^{lra}) \\ &+ \text{RRAscore}(u^{rra}, v^{rra}) \\ &+ \text{CIAscore}(u^{lcia}, v^{lcia}, u^{rcia}, v^{rcia}),\end{aligned}$$

and the valid pairing with the maximum score is finally considered as the solution of the matching problem. Since the enumeration of the different pairings results in a small number of valid pairings, this solution can be determined in a few seconds by a brute-force search, which compares the scores of all valid pairings. In the case where the optimal solution is not unique, we consider the optimal solution that contains the least number of branches (i.e. the first one containing the most nodes v equal to $\varnothing$). In the following, we detail the score evaluation for each artery.

Renal arteries score. The RAs branch off from the aorta to the left and right as illustrated in Figure 7. For this reason, we first impose that the global and local directions of the branch corresponding to the left (resp. right) RA points to the left (resp. right) :

$$\text{angle}_{x,y}\left(\mathbf{d}_{glob}(u^{lra}, v^{lra}), \mathbf{d}^1\right) < \frac{\pi}{3} \quad \text{and} \quad \text{angle}_{x,y}\left(\mathbf{d}_{loc}(u^{lra}, v^{lra}), \mathbf{d}^1\right) < \frac{\pi}{3} \tag{12}$$

$$\text{angle}_{x,y}\left(\mathbf{d}_{glob}(u^{rra}, v^{rra}), \mathbf{d}^2\right) < \frac{\pi}{3} \quad \text{and} \quad \text{angle}_{x,y}\left(\mathbf{d}_{loc}(u^{rra}, v^{rra}), \mathbf{d}^2\right) < \frac{\pi}{3} \tag{13}$$

with $\mathbf{d}^1 = (1,0,0)^T$ and $\mathbf{d}^2 = (-1,0,0)^T$. The score of the left (resp. right) RA then corresponds to the length of the branch in the left (resp. right) direction:

$$\text{LRAscore} = \begin{cases} x^+(u^{lra}, v^{lra}) & \text{if } u^{lra}, v^{lra} \neq \varnothing \text{ and (12)} \\ 0 & \text{otherwise,} \end{cases}$$

and

$$\text{RRAscore} = \begin{cases} x^-(u^{rra}, v^{rra}) & \text{if } u^{rra}, v^{rra} \neq \varnothing \text{ and (13)} \\ 0 & \text{otherwise.} \end{cases}$$

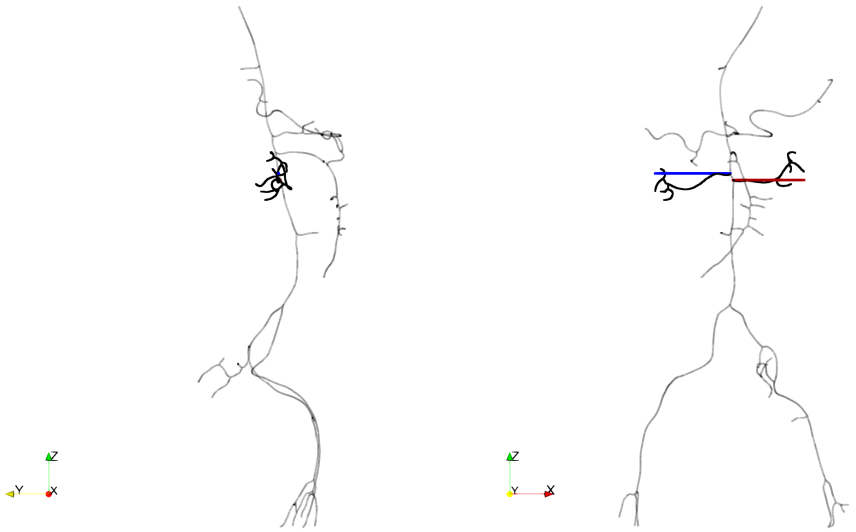

Fig. 7 Example illustrating the RAs score evaluation: vascular tree (grey), branches corresponding to the RAs (black), $x^-(u^{rra}, v^{rra})$ (blue) and $x^+(u^{lra}, v^{lra})$ (red).

Common iliac arteries score. The CIAs originate from the aortic bifurcation and run in the left-inferior and right-inferior directions as shown in Figure 8. We therefore impose that the global direction of the branch corresponding to the left (resp. right) CIA is oriented in the left-inferior (resp. right-inferior) direction:

$$\text{angle}_{x,z}\left(\mathbf{d}_{glob}(u^{lcia}, v^{lcia}), \mathbf{d}^1\right) < \frac{\pi}{4} \quad \text{and} \quad \text{angle}_{x,z}\left(\mathbf{d}_{glob}(u^{rcia}, v^{rcia}), \mathbf{d}^2\right) < \frac{\pi}{4} \qquad (14)$$

with $\mathbf{d}^1 = (1,0,-1)^T$ and $\mathbf{d}^2 = (-1,0,-1)^T$. The score of the left (resp. right) CIA then corresponds to the branch length in the left (resp. right) and inferior directions. However, as the RA score considers the branch length in only one direction, we weight the CIA score by taking the diagonal formed by these two lengths: $\sqrt{(x^+(u^{lcia}, v^{lcia}))^2 + (z^-(u^{lcia}, v^{lcia}))^2}$ and $\sqrt{(x^-(u^{rcia}, v^{rcia}))^2 + (z^-(u^{rcia}, v^{rcia}))^2}$ for the left and right CIAs, respectively. Moreover, we add the contribution of the aorta: $z^+(u^{lcia}, n^{aorta})$ with $n^{aorta} = u^{max}$ if $u^{lcia} \neq u^{max}$ and

$n^{aorta} = v^{max}$ otherwise, in order to find the bifurcation that forms the largest inverted "Y" in the vascular tree. The score of the CIAs is finally defined by

$$\text{CIAscore} = \begin{cases} \sqrt{(x^+(u^{lcia},v^{lcia}))^2 + (z^-(u^{lcia},v^{lcia}))^2} & \text{if } u^{lcia},v^{lcia},u^{rcia},v^{rcia},n^{aorta} \neq \varnothing \\ \quad + \sqrt{(x^-(u^{rcia},v^{rcia}))^2 + (z^-(u^{rcia},v^{rcia}))^2} & \text{and (14)} \\ \quad + z^+(u^{lcia},n^{aorta}) & \\ 0 & \text{otherwise.} \end{cases}$$

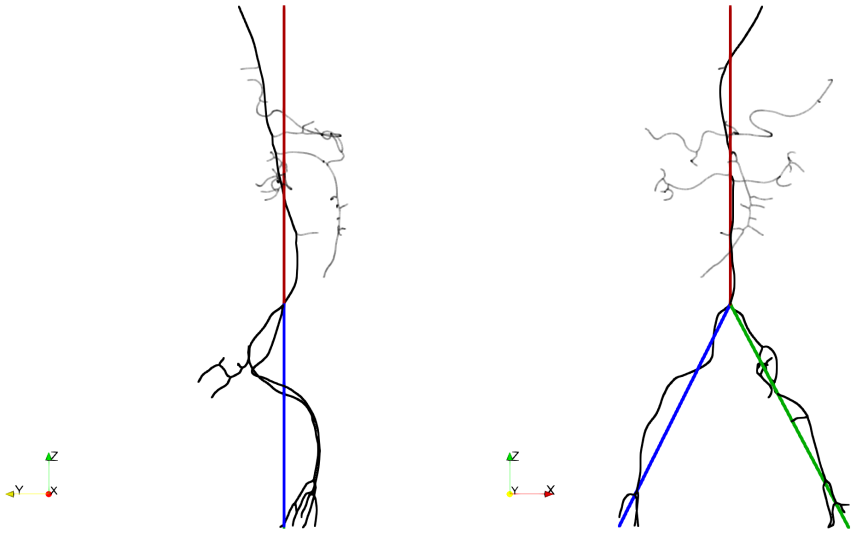

Fig. 8 Example illustrating the CIAs score evaluation: vascular tree (grey), branches corresponding to the aorta and CIAs (black), $\sqrt{(x^-(u^{rcia},v^{rcia}))^2 + (z^-(u^{rcia},v^{rcia}))^2}$ (blue), $\sqrt{(x^+(u^{lcia},v^{lcia}))^2 + (z^-(u^{lcia},v^{lcia}))^2}$ (green) and $z^+(u^{lcia},n^{aorta})$ (red).

Superior mesenteric artery score. The SMA leaves the aorta in the anterior direction and then tends to the inferior direction as illustrated in Figure 9. For this reason, we first impose that the local direction of the branch corresponds to the anterior direction:

$$\text{angle}_{x,y}\left(\mathbf{d}_{loc}(u^{sma},v^{sma}),\mathbf{d}\right) < \frac{\pi}{3} \tag{15}$$

with $\mathbf{d} = (0,-1,0)^T$. The score is then given by the length of the branch in the anterior direction $y^-(u^{sma},v^{sma})$. In addition, if the local direction verifies

$$\text{angle}_{x,y}\left(\mathbf{d}_{loc}(u^{sma},v^{sma}),\mathbf{d}\right) < \frac{\pi}{6} \tag{16}$$

with $\mathbf{d} = (0,-1,0)^T$, or if the main length of the branch corresponds to the anterior or inferior direction:

$$\max\left(y^-(u^{sma},v^{sma}),z^-(u^{sma},v^{sma})\right) > \max\left(x^+(u^{sma},v^{sma}),x^-(u^{sma},v^{sma})\right), \tag{17}$$

then we add the contribution of the branch length in the inferior direction $z^-(u^{sma}, v^{sma})$. This notably allows to contrast the score of the SMA with that of the CA. The SMA score is thus defined by

$$\text{SMAscore} = \begin{cases} y^-(u^{sma}, v^{sma}) + z^-(u^{sma}, v^{sma}) & \text{if } u^{sma}, v^{sma} \neq \varnothing \text{ and (15) and ((16) or (17))} \\ y^-(u^{sma}, v^{sma}) & \text{if } u^{sma}, v^{sma} \neq \varnothing \text{ and (15)} \\ 0 & \text{otherwise.} \end{cases}$$

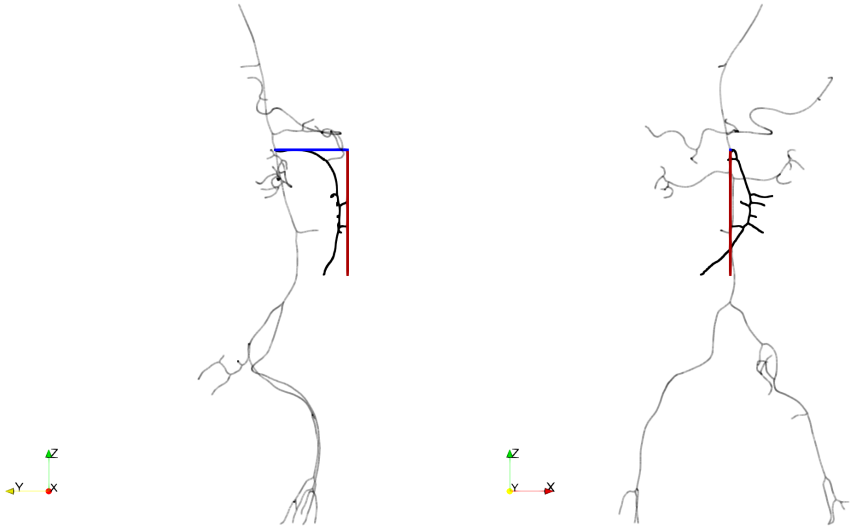

Fig. 9 Example illustrating the SMA score evaluation: vascular tree (grey), branch corresponding to the SMA (black), $y^-(u^{sma}, v^{sma})$ (blue) and $z^-(u^{sma}, v^{sma})$ (red).

Celiac artery score. The CA starts from the aorta in the anterior direction and then tends to go to the left and right as shown in Figure 10. As for the SMA, we impose that the local direction of the branch is directed towards the anterior direction:

$$\text{angle}_{x,z}(\mathbf{d}_{loc}(u^{ca}, v^{ca}), \mathbf{d}) < \frac{\pi}{3} \tag{18}$$

with $\mathbf{d} = (0, -1, 0)^T$, and the score is given by the length of the branch in the anterior direction $y^-(u^{ca}, v^{ca})$. However, the additional contribution is based on the branch lengths in the left $x^+(u^{ca}, v^{ca})$ and right $x^-(u^{ca}, v^{ca})$ directions to contrast with the SMA score. This contribution is added only if the local direction verifies:

$$\text{angle}_{x,z}(\mathbf{d}_{loc}(u^{ca}, v^{ca}), \mathbf{d}) < \frac{\pi}{6}, \tag{19}$$

with $\mathbf{d} = (0, -1, 0)^T$, or if the main length of the branch corresponds to the anterior, left or right direction:

$$\max\left(y^+(u^{ca}, v^{ca}), x^+(u^{ca}, v^{ca}), x^-(u^{ca}, v^{ca})\right) > z^-(u^{ca}, v^{ca}). \tag{20}$$

However, as the SMA additional contribution considers only one direction, the contribution of the branch lengths in the left and right directions is divided by two in order to weight the score. The score of the CA is finally given by

$$\text{CAscore} = \begin{cases} y^-(u^{ca},v^{ca}) + \dfrac{x^+(u^{ca},v^{ca}) + x^-(u^{ca},v^{ca})}{2} & \text{if } u^{ca},v^{ca} \neq \varnothing \text{ and (18) and ((19) or (20))} \\ y^-(u^{ca},v^{ca}) & \text{if } u^{ca},v^{ca} \neq \varnothing \text{ and (18)} \\ 0 & \text{otherwise.} \end{cases}$$

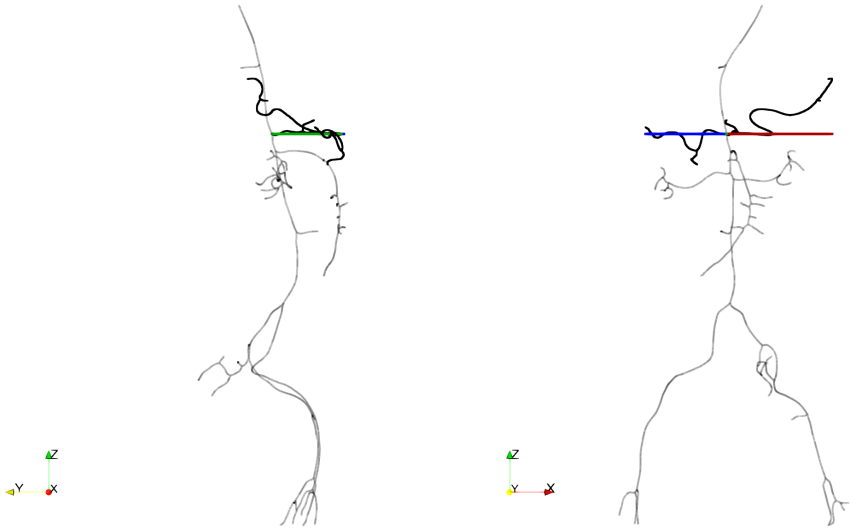

Fig. 10 Example illustrating the CA score evaluation: vascular tree (grey), branch corresponding to the CA (black), $x^-(u^{ca},v^{ca})$ (blue), $x^+(u^{ca},v^{ca})$ (red) and $y^-(u^{ca},v^{ca})$ (green).

2.2.4 Detection of non-anatomic branches

Since the aorta is not perfectly cylindrical, the vascular tree may contain non-anatomic branches resulting from small bumps on the surface of the aorta. As shown in Figure 11, these branches are small and do not correspond to any artery. For these reasons, we check the length of the branches $\{(u^{ca},v^{ca}),\ldots,(u^{rcia},v^{rcia})\}$ to detect potential non-anatomic branches. If the length of a branch (u,v) is less than 3 times the radius r of the aorta at node u or if the length is less than 20 mm plus the radius r:

$$\text{length}(u,v) < 3r \quad \vee \quad \text{length}(u,v) < r + 20 \text{ mm}, \tag{21}$$

then a warning is sent to signal that this branch is small and may correspond to a non-anatomic branch. Condition (21) involves two parameters: the minimum relative length of the branch ($3r$) and the minimum absolute length of the branch ($r+20$ mm). These parameters were determined according to Figure 12 in order to be large enough to detect non-anatomic branches.

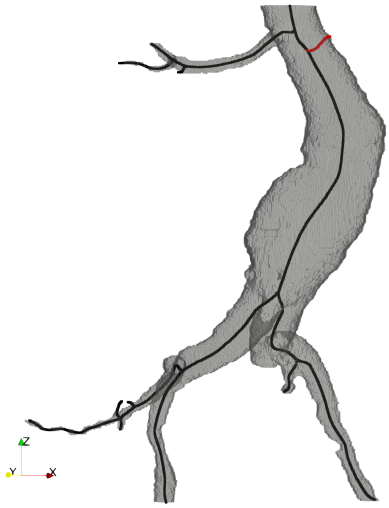

Fig. 11 Example of non-anatomic branch: segmentation (grey), vascular tree (black) and non-anatomic branch (red).

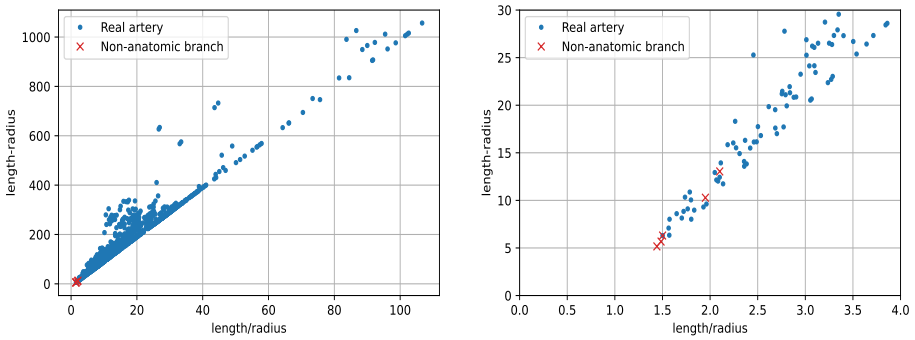

Fig. 12 Left: statistics used to determine the parameters involved in condition (21). Right: zoom of the left figure. These statistics were computed from the 239 segmentations of the dataset.

2.3 Decision rule-based algorithm

Definition 8 *Given a branch starting from b and going to n^1, we call primary branch the path $(b, n^1, ..., n^k)$ where n^k denotes the first bifurcation or leaf encountered. Let's p^4 be the fourth point of the primary branch.*

Once we had the pairing with the highest score, we looked for one extra left and one extra right renal artery among the branches that were not already identified by the matching algorithm. Among the remaining bifurcation points on the aorta, we kept those that were

Condition	Total number of branches	Non-anatomic branches
1	21	19
2	3	3
3	2	2
4	11	11
5	2	2

Table 2 Distribution of the branches according to the 5 conditions described in Section 2.3.

above the highest supra-renal artery and less than 20 mm far and those that were above the aortic bifurcation and more than 80 mm far, along the vascular tree. We then removed branches that went to the front of the body, that is branches with a local direction such that:

$$\text{angle}_{x,y}\left(\mathbf{d}_{loc}(b,p^4),\mathbf{d}\right) > \frac{3\pi}{4} \tag{22}$$

with $\mathbf{d} = (0,-1,0)^T$.

For the left renal artery (resp. right) we kept branches whose local direction respected:

$$\text{angle}_{x,y}\left(\mathbf{d}_{loc}(b,p^4),\mathbf{d}\right) < \frac{\pi}{3} \tag{23}$$

with $\mathbf{d} = (1,0,0)^T$ (resp. $\mathbf{d} = (-1,0,0)^T$).

For each candidate we had the following indicator:

$$I_{\text{C}} = \begin{cases} x^+(b,p^4) - |b_z - u_z^{rra}| & \text{for left RA if } u^{rra} \neq \varnothing \\ x^+(b,p^4) & \text{for left RA if } u^{rra} = \varnothing \\ x^-(b,p^4) & \text{for right RA.} \end{cases} \tag{24}$$

What was left to determine was if the remaining branches fitted other exclusion criteria. We rejected a branch in the following cases:

- the primary branch ended with a leaf, $\text{dist}(b,n^k) < 22$ mm and $\dfrac{I_{\text{C}}}{I_{\text{RA}}} \leq 0.94$,
- the primary branch ended with a bifurcation node and $\text{dist}(b,n^k) < 15$ mm,
- $I_{\text{C}} \leq -19$,
- $0 \leq I_{\text{C}} \leq 15$, $\text{dist}(b,n^k) < 25$ mm and $\dfrac{I_{\text{C}}}{I_{\text{RA}}} \leq 0.2$,
- $\dfrac{I_{\text{C}}}{I_{\text{RA}}} \geq 1$,

where I_{RA} is the indicator (24) of the left (resp. right) renal artery identified by the matching algorithm. If more than one branch remained, we kept the longest. The distribution of the branches according to the 5 conditions can be found in Table 2. All the thresholds were determined by experience on our dataset.

Finally we checked the euclidean distance between the lowest renal artery and the aortic bifurcation: if it was less than 75 mm, a warning was sent to ask for validation.

3 Results

The accuracy of the proposed method was evaluated by comparing the results with manual annotations provided by human experts. A result is considered correct if the branches

annotated by the method correspond to the manually annotated branches and incorrect otherwise. Among the 239 segmentations, 213 cases (89.1%) were correctly annotated by our automatic branch detection method. In the remaining 26 cases, at least one of the arteries was misidentified. We detail the reason for these errors in the following.

		Accuracy
Common iliac arteries		97.9%
Celiac and superior mesenteric arteries		97.5%
Renal arteries (cases without polar renal artery)		94.4%
Renal arteries (cases with polar renal arteries)	Principal renal artery	95.8%
	Polar renal artery	70.8%
Infrarenal zone		94.6%
All arteries		89.1%

Table 3 Summary of the results of the proposed method over the 239 segmentations of the dataset.

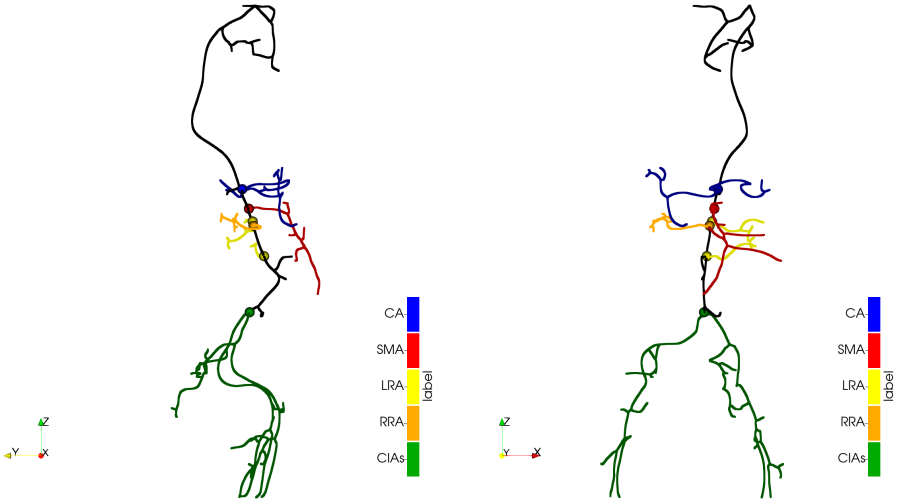

Fig. 13 Example of vascular tree correctly annotated: vascular tree (black), branches corresponding to the CA (blue), SMA (red), left RAs (yellow), right RA (orange) and CIAs (green).

Common iliac arteries. The CIAs and the corresponding aortic bifurcation were correctly identified by the matching algorithm in 234 cases (97.9%). Of the incorrect cases, 3 are due to the presence of non-anatomic bifurcations as illustrated in Figure 14. These ones result from a contact point between the CIAs and divide the left or right CIA into two separate branches. The vascular tree then no longer properly represents the topology of the arterial system, and the matching algorithm identified the longest branches since they lead to a higher score. These branches represent a large portion of the left and right CIAs, respectively, but they do not originate from the aortic bifurcation. In the 2 other cases, the segmentation was cut just below the aortic bifurcation. It results that the CIAs are very short

(less than 33 mm), and the matching algorithm identified a bifurcation with longer branches. In theses two cases, a warning suggesting to check the result was raised because of the small distance between the wrong aortic bifurcation and the other bifurcations.

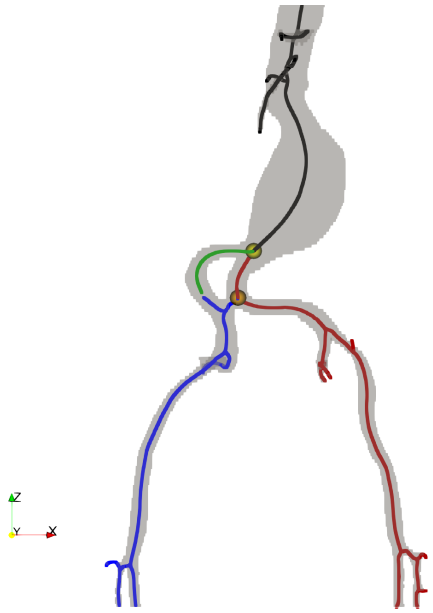

Fig. 14 Example of non-anatomic bifurcation: segmentation (grey), vascular tree (black), branch corresponding to the left CIA (red), branches corresponding to the right CIA (blue and green), aortic bifurcation (yellow) and non-anatomic bifurcation (orange).

Celiac and superior mesenteric arteries. The CA and SMA were correctly identified in 233 cases (97.5%). Of the cases in which at least one of the two arteries was misidentified, 2 are due to the presence of non-anatomic bifurcations occurring when the SMA descends and comes too close to the aorta. As for the CIAs, the matching algorithm identified the branch originating from the non-anatomic bifurcation and corresponding to the longest part of the SMA. In 3 other cases, the segmentation did not contain CA or SMA, but a non-anatomic branch was identified as a CA or SMA because it leads to a higher score. Finally, the last incorrect case is due to a SMA which is oriented to the left and was mistaken for a left RA.

Renal arteries. Over the 215 cases without polar RAs, the method correctly identified the RAs in 203 cases (94.4%). On the one hand, the matching algorithm wrongly identified the RAs in 6 cases. Of the incorrect cases, 4 are due to the presence of non-anatomic bifurcations or non-anatomic branches, 1 is due to a RA that points to the anterior direction, and 1 is due to a SMA oriented to left and mistaken for a left RA. On the other hand, the decision-rule based algorithm wrongly identified non-anatomic branches as additional RAs in 6 cases. These branches have the same characteristics (position, angle, length) as a small RA and could not be distinguished from a real one as shown in Figure 15.

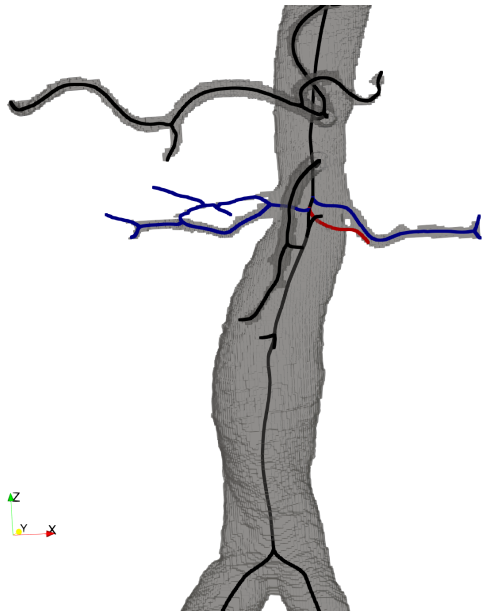

Fig. 15 Example of non-anatomic branch identified as a second left RA: segmentation (grey), vascular tree (black), RAs (blue) and non-anatomic branch (red).

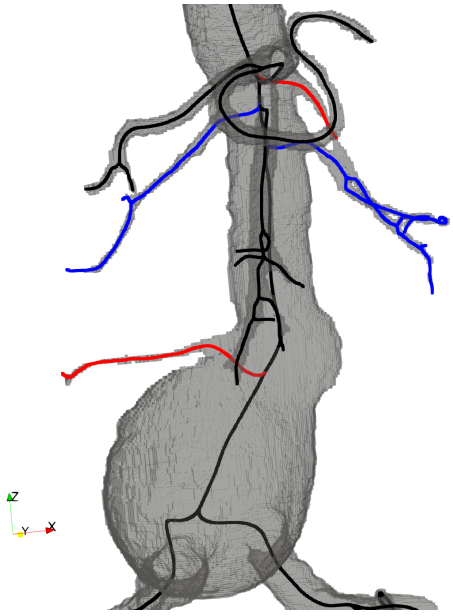

Fig. 16 Example of additional RAs identified as non-anatomic branches: segmentation (grey), vascular tree (black), RAs correctly identified (blue) and RAs wrongly identified (red).

Over the 24 cases with polar RAs, the method correctly identified the principal and polar RAs in 16 cases (66.7%). In all cases, a first (principal or polar) RAs was correctly identified by the matching algorithm. Of the cases where the second RAs were not identified, 1 is due to very short CIAs. As a result, the second left RAs was already identified as the left CIA by the matching algorithm. In addition, the decision-rules based algorithm missed to identify the second left or right RA in 7 case. The three main reasons were an angle that did not fit in the predetermined interval, an artery that was too close to the aortic bifurcation or one that was too short (less than 25 mm) as illustrated in Figure 16.

Infrarenal zone. The infrarenal zone is defined as the portion of the aorta between the lowest RA and the aortic bifurcation. The lowest RA was well identified in 229 cases (95.8%). Combined with the results concerning the aortic bifurcation, we recovered the infrarenal zone in 226 cases (94.6%).

4 Discussion

The previous results show that the errors of our method come mainly from the presence of non-anatomic bifurcations, non-anatomic branches, and arteries that do not have the direction they are supposed to have. In particular, we identified 3 cases where a non-anatomic bifurcation was mistaken for the aortic bifurcation. However when we removed this non-anatomic bifurcation from the vascular tree, the aortic bifurcation was correctly identified. Similarly, if the non-anatomic branches are removed from the vascular trees, our method will no longer identify them. This means that any improvement in the quality of both the segmentation and the vascular tree could lead to better results. Nevertheless, our method is robust with respect to non-anatomic branches. Indeed, there were a total of 185 non-anatomic branches in the 239 segmentations, and only 18 (5 for the matching algorithm and 13 for the decision-rules based algorithm) led to errors, i.e. 9.7%. Regarding the direction of the branches, we have chosen large angle intervals to prevent this kind of error as much as possible. However, if an artery has a very atypical angle, our method will fail to identify it.

In this work, the vascular trees were extracted from the full segmentation, that is lumen and thrombus. Nevertheless, our method can also be applied to vascular trees computed only from the lumen. However, these vascular trees contain more non-anatomic bifurcations and non-anatomic branches, as shown in Figure 17. It follows that our method makes more errors. For example, a non-anatomic branch was identified as a second RA in 12 cases, against 7 cases for the full segmentation. In addition, the vascular trees extracted from the lumen do not contain the aortic bifurcation in 5 cases. This is due to either the absence of a CIA in the lumen segmentation or the presence of an endoprothesis in the post-operative scan, as illustrated in Figure 17.

Although an error on the aortic bifurcation does not necessarily lead to errors on the other branches, we check the distance between the lowest RA and the aortic bifurcation to detect potential errors. A warning was raised in 6 cases because of the small distance between the aortic bifurcation and the other bifurcations. In 2 cases the aortic bifurcation was wrongly identified, in 2 other the distance was short because of a low polar renal artery. In the 2 last cases there was no renal artery found nor segmented. We expose the distance between the lowest renal artery and the aortic bifurcation for all the segmentations of the dataset in Figure 18.

Fig. 17 Comparison of vascular trees extracted from the lumen (left) and full segmentations (right): segmentation (grey), vascular tree (black) and aortic bifurcation (green).

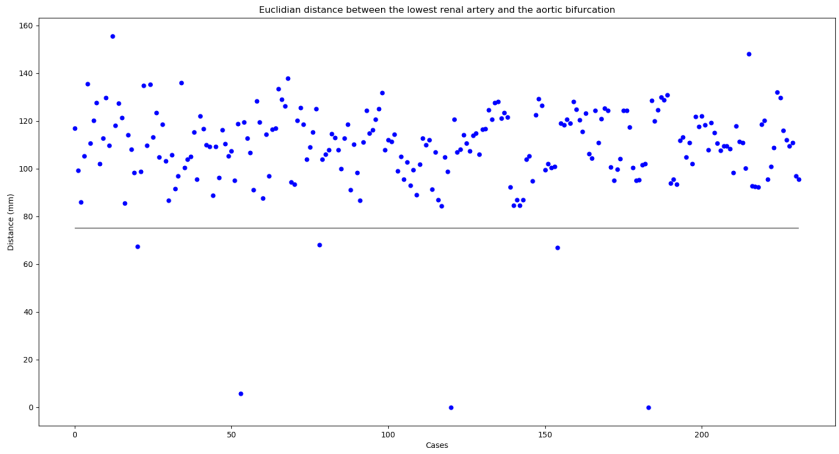

Fig. 18 Distance between the identified lowest renal artery and the aortic bifurcation. The black line represents the threshold value at 75mm. The separation between rising or not a warning is clear.

The method proposed in [7] is evaluated by

$$\text{the precision rate} = \frac{TP}{TP+FP}\% \quad \text{and} \quad \text{the recall rate} = \frac{TP}{TP+FN}\%,$$

where TP denotes the number of branches correctly labeled, FP denotes the number of branches incorrectly labeled and FN denotes the number of branches that should be labeled but not labeled. In comparison with our approach, those rates were 94.7% and 65% for the

CIAs while we obtain 97.9% and 100% respectively. Similarly, for the CA and SMA, our method results in precision and recall rates of 97.9% and 99.6% against at most 80.8% and 89.1%. Concerning the RAs, the precision and recall rates were 63.3% and 41.3%, while we achieve 95% and 96% respectively. Our method was not only tested on a larger dataset, it also showed better precision and recall.

5 Conclusions

In this work, we have presented a new method to automatically identify different arteries present in an abdominal aortic segmentation. In this approach, the arterial system is first represented by the vascular tree extracted from the full segmentation, that is lumen and thrombus. Then, a matching algorithm finds the branches of the vascular tree that best anatomically match the different arteries located along the aorta: CA, SMA, RAs, and CIAs. A decision rule-based algorithm finally looks for the presence of additional RAs to obtain the complete description of the arterial system.

The method has been evaluated on 239 segmentations from 102 different patients. The results demonstrate the accuracy of the method, capable of delivering an error of less than 2.5% for the identification of the CA and SMA, 2.1% for the CIAs, 8.4% for the RAs, 5.4% for the infrarenal zone and 10.9% for all arteries. In addition, we have seen that these errors come mainly from the presence of non-anatomic bifurcations or non-anatomic branches, so any improvement in the quality of both the segmentation and the vascular tree could lead to better results.

The accuracy of the method could be further improved by exploiting more information from branch diameters. These could notably avoid confusing the CIAs with smaller RAs. Moreover, the diameters could also be used to identify the aorta, allowing to extend the method to vascular trees that do not contain the aortic bifurcation, for example, when the segmentation is cut in the middle of the sac.

Author contribution

Method: Sébastien Riffaud (Matching algorithm), Gwladys Ravon (Decision rule-based algorithm) ; Supervision: Florian Bernard, Angelo Iollo ; Results: Sébastien Riffaud, Gwladys Ravon, Thibault Allard, Caroline Caradu ; Initial draft writing: Sébastien Riffaud, Gwladys Ravon ; All authors contribute to editing and improving the manuscript.

Conflict of interest

The authors declare that they have no conflict of interest.

References

1. Caradu, C., Spampinato, B., Vrancianu, A.M., Bérard, X., Ducasse, E.: Fully automatic volume segmentation of infrarenal abdominal aortic aneurysm computed tomography images with deep learning approaches versus physician controlled manual segmentation. Journal of Vascular Surgery **74**(1), 246–256 (2021)
2. Chaikof, E.L., Dalman, R.L., Eskandari, M.K., Jackson, B.M., Lee, W.A., Mansour, M.A., Mastracci, T.M., Mell, M., Murad, M.H., Nguyen, L.L., et al.: The Society for Vascular Surgery practice guidelines on the care of patients with an abdominal aortic aneurysm. Journal of vascular surgery **67**(1), 2–77 (2018)

3. Dehmeshki, J., Amin, H., Ebadian-Dehkordi, M., Jouannic, A., Qanadi, S.: Automatic detection, segmentation and quantification of abdominal aortic aneurysm using computed tomography angiography. Proc. Med. Image Understand. Anal pp. 32–36 (2009)
4. Elattar, M., Wiegerinck, E., van Kesteren, F., Dubois, L., Planken, N., Vanbavel, E., Baan, J., Marquering, H.: Automatic aortic root landmark detection in CTA images for preprocedural planning of transcatheter aortic valve implantation. The international journal of cardiovascular imaging **32**(3), 501–511 (2016)
5. Lalys, F., Esneault, S., Castro, M., Royer, L., Haigron, P., Auffret, V., Tomasi, J.: Automatic aortic root segmentation and anatomical landmarks detection for TAVI procedure planning. Minimally invasive therapy & allied technologies **28**(3), 157–164 (2019)
6. Nordon, I.M., Hinchliffe, R.J., Loftus, I.M., Thompson, M.M.: Pathophysiology and epidemiology of abdominal aortic aneurysms. Nature reviews cardiology **8**(2), 92–102 (2011)
7. Oda, M., Hoang, B.H., Kitasaka, T., Misawa, K., Fujiwara, M., Mori, K.: Automated anatomical labeling method for abdominal arteries extracted from 3D abdominal CT images. In: Medical Imaging 2012: Image Processing, vol. 8314, p. 83142F. International Society for Optics and Photonics (2012)
8. Tahoces, P.G., Santana-Cedrés, D., Alvarez, L., Alemán-Flores, M., Agustín, T., Carmelo, C., Carreira, J.M.: Automatic detection of anatomical landmarks of the aorta in CTA images. Medical and Biological Engineering and Computing **58**(5), 903–919 (2020)

Sébastien Riffaud is a postdoctoral researcher at Inria - Bordeaux Sud-Ouest in Memphis team. He graduated with a Ph.D. in applied mathematics and scientific computing from University of Bordeaux in 2020. His current research focuses on the development of efficient and accurate methods for modeling blood flow in the aorta.

Gwladys Ravon completed a PhD in applied mathematics at the University of Bordeaux. The subject mixed inverse problems and cardiac electrophysiology. She has currently a post-doctoral position at Inria Bordeaux Sud-Ouest in Memphis Team. Her main research topic is applied mathematics to medicine and health care.

Thibault Allard graduated from University of Technology of Troyes as materials engineer. After getting an experience in big companies such as l'Oreal and an MBA in Data Science from MBA ESG, he joined Nurea as Data Scientist. He's very enthusiastic about new technologies and consider that artifical intelligence is a great resource that can help improving patient care.

Florian Bernard completed a PhD in applied mathematics at University of Bordeaux and a PhD in fluid dynamics at Politecnico di Torino in 2015. He's now CEO of Nurea, a company dedicated to the development of decision making support software for physicians to improve diagnostic, follow up and pronostic of cardiovascular diseases.

Angelo Iollo is professor of Applied Mathematics at the University of Bordeaux and head of team Memphis at Inria, the national institute for applied mathematics and computer science.

Dr. Caroline Caradu is a M.D. Ph.D. working as a vascular surgeon at the University Hospital of Bordeaux. Her research interests include the endovascular treatment of complex aortic aneurysms, the use of artificial intelligence in the treatment of vascular pathologies, aortic infections, and the role of endothelial cell dysfunction in the pathophysiology of critical limb ischemia.